Icarus 401 (2023) 115616

Contents lists available at ScienceDirect

Icarus

journal homepage: www.elsevier.com/locate/icarus

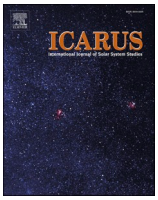

Micro-meteoroids impact vaporization as source for Ca and CaO exosphere along Mercury's orbit

M. Moroni [a,*], A. Mura [a], A. Milillo [a], C. Plainaki [b], V. Mangano [a], T. Alberti [a,c], N. Andre [d], A. Aronica [a], E. De Angelis [a], D. Del Moro [a,e], A. Kazakov [a], S. Massetti [a], S. Orsini [a], R. Rispoli [a], R. Sordini [a]

[a] Istituto Nazionale di Astrofisica – Istituto di Astrofisica e Planetologia Spaziali (INAF – IAPS), Rome, Italy
[b] Agenzia Spaziale Italiana (ASI), Rome, Italy
[c] Istituto Nazionale di Geofisica e Vulcanologia, Rome, Italy
[d] Research Institute in Astrophysics and Planetology (IRAP), Toulose, France
[e] Department of Physics, University of Rome Tor Vergata, Italy

ARTICLE INFO

Keywords:
Mercury atmosphere
Interplanetary dust
Impact processes

ABSTRACT

The study of the micro-meteoroid environment is relevant to planetary science and space weathering of airless bodies, as the Moon or Mercury. In fact, the meteoroids hit directly the surfaces producing impact debris and vapor, thus contributing to shape the exosphere of the planet. This work is focused on the study and modelling of the Mercury's Ca exosphere formation through the process of Micro-Meteoroids Impact Vaporization (MMIV). The MESSENGER/NASA mission provided measurements of Mercury's Ca exosphere, allowing the study of its configuration and its seasonal variations. The observed Ca exhibited very high energies, with a scale height consistent with a temperature $>$ 50,000 K, originated mainly on the dawn-side of the planet. It was suggested that the originating process is due to MMIV, but previous estimations were not able to justify the observed intensity and energy. We investigate the possible pathways to produce the high energy observed in the Ca exosphere and discuss about the generating mechanism. The most likely origin may be a combination of different processes involving the release of atomic and molecular surface particles. We use the exospheric Monte Carlo model by Mura et al. (2007) to simulate the 3-D spatial distribution of the Ca-bearing molecule and atomic Ca exospheres generated through the MMIV process, and we show that their morphology and intensity are consistent with the available MESSENGER observations if we consider a cloud quenching temperature $<$ 3750 K. The results presented in this paper can be useful in the exospheric studies and in the interpretation of active surface release processes, as well as in the exosphere observations planning for the ESA-JAXA BepiColombo mission that will start its nominal mission phase in 2026.

1. Introduction

Exospheres are optically thin shells surrounding planetary bodies where particle trajectories are predominantly guided by gravity rather than by collisions. Mercury has a surface-bounded exosphere continuously refilled and depleted through processes acting both on the surface and within the planet's environment (Milillo et al., 2005, 2020). Such processes are strongly driven by external factors such as the solar irradiance, the solar wind and the micrometeoroid flux precipitating on the surface, as well as the planet's physical and chemical properties. As a consequence, the study of the generation mechanisms and of the Hermean exospheric composition can provide crucial insights for understanding the nature of the planetary environment, the escape (or loss) rates of exospheric species from the planet as well as the planet's evolution.

The surface release processes that are generally considered as possible responsible for the generation of the Mercury's exosphere are mainly (Milillo et al., 2005; Seki et al., 2015 *and references therein):* Photon-Stimulated Desorption, resulting from the desorption of neutrals or ions induced by photon bombardment onto the surface; Thermal Desorption, inducing the release of absorbed atoms from the surface via thermal energy increase; Ion Sputtering, caused by solar wind and/or

* Corresponding author.
E-mail address: martina.moroni@inaf.it (M. Moroni).

https://doi.org/10.1016/j.icarus.2023.115616
Received 24 October 2022; Received in revised form 20 March 2023; Accepted 8 May 2023
Available online 9 May 2023

planetary ions precipitating onto the surface; and MicroMeteoroid Impact Vaporization (MMIV), producing surface release due to meteoroids hitting directly the surface, like impact debris, melt and vapor, thus contributing to the planet's exosphere. Volatiles and refractory elements of the exosphere are subject to different loss and source processes. Generally speaking, for light gases the gravitational escape dominates and photoionization and electron impact ionization are important loss mechanisms, so that volatiles are sensitive to the intense thermal and UV radiation due to Mercury's proximity to the Sun. On the contrary, refractories are in general responsive only to the most energetic processes like MMIV and ion sputtering (Milillo et al., 2020 *and references therein)*.

The NASA/MESSENGER (MErcury Surface, Space ENvironment, GEochemistry, and Ranging) mission visited Mercury in the period 2008–2015, provided in-situ measurements of Mercury's exosphere and permitted the study of the seasonal variations of metals like Mg (Merkel et al., 2017) and Ca (Burger et al., 2014). The present work is focused on the study of Mercury's Ca and CaO exospheres generated through MMIV. Following the approach in Plainaki et al. (2017), we modify the exospheric Monte Carlo model by Mura et al. (2007) with the scope to provide a refined 3-D density distribution of Mercury's Ca and CaO exospheres at different True Anomaly Angles (TAA) (angle between perihelium and the planet as seen from the Sun).

The Monte Carlo model presented here includes a combination of different exospheric source and loss processes, such as the release of atomic and molecular surface particles and the photodissociation of exospheric molecules and provides simulations of distribution of atomic and molecular exospheric components.

The paper is organized as follows: in Section 2 we provide details on the physical processes considered within our model whereas in Section 3 we describe the model and assumptions. In Section 4, we discuss the morphology of Mercury's Ca and CaO exospheres at different TAA as obtained by our model and we compare our results with the available MESSENGER/MASCS observations. The conclusions are given in Section 5, drawing a roadmap for future analysis and observations, with the aim to improve our knowledge of the MMIV process at Mercury.

2. MicroMeteoroid impact vaporization

The particles of small sizes (< 100 μm) impact into the regolith of Mercury at a mean velocity of 30 km/s (Cintala, 1992) and we can observe from Pokorný et al. (2018) that there is also a less frequent component of fast particles with velocity in the range 80–110 km/s. Larger impactors with size >2 cm arrive with a much broader impact velocity distribution at Mercury, ranging from 4 to around 40 km/s (Marchi et al., 2005), causing local enhancement of exospheric density. Nevertheless, the larger particles are likely of little significance for the study of the permanent exosphere content because they can produce significant local enhancements but are infrequent (Mangano et al., 2007), while the exosphere is continuously replenished.

Exospheric formation through MMIV process depends both on the impact velocity and on the directionality of incoming flux with respect to the planet's motion. The bombardment of Mercury's surface by micro-meteoroids derives from different sources, as Jupiter Family Comets (JFCs), Main Belt Asteroids (MBA), Halley Type and Oort Cloud Comets (HTCs and OCCs) (Pokorný et al., 2018). We know that MBA meteoroids dominate the flux at Earth, in comparison to particles from cometary sources (Ceplecha, 1992), but meteoroids originating from short period comets, as JFCs, dominate the inner Solar System (Nesvorný et al., 2010, 2011).

2.1. Ca exosphere generation

Whereas the Na component of Mercury's exosphere has been regularly observed, the Ca detections are much more limited in time because the emission is fainter and at a wavelength that is more difficult to observe from the Earth than the Na D-lines. Differently from other exospheric species like Na, refractories species like Ca are expected to be released from the surface by more energetic processes like MMIV and/or ion sputtering (Killen et al., 2010, Wurz and Lammer, 2003). Experimental works (Kurosawa, 2012) reproduced silicate vaporization after impact with the aim to understand energy process during impacts. The measured temperature of the shock-induced cloud just after impact (the first 100 ns) was estimated to be between 15.000 K and 27.000 K. The temperature and pressure quickly decrease during adiabatic expansion of the cloud reaching a quenching temperature of the order of 4000 K.

Mercury's Ca exosphere was discovered through ground-based Keck telescope observations of the Ca emission line at 422.7 nm (Bida et al., 2000) and later detected in-situ by the Ultraviolet and Visible Spectrometer (UVVS), one sensor of the MASCS instrument (McClintock and Lankton, 2007) onboard MESSENGER spacecraft (Solomon and Anderson, *2018*). During MESSENGER's flybys of Mercury, the UVVS made the first high-spatial-resolution observations of exospheric Ca at Mercury that exhibited very high energies, with a scale height consistent with a temperature up to 50,000 K. Burger et al. (2014) simulated these data with a model of exospheric source processes to reproduce this persistent and extremely hot Ca exosphere that is seen almost exclusively on the dawn-side of the planet and with a seasonally, not sporadically, variable content.

The origin of this high-energy, asymmetrically distributed population still needs to be fully explained. Killen (2016) examined different possible pathways responsible for ejecting Ca from Mercury's surface to the exosphere. To explain the observed Ca energization, ion sputtering is not considered as the primary source process for Ca: in fact, thought it could explain the high energy of observed Ca, it could not reproduce the measured spatial and temporal variation. The collisions between meteoroids and planetary surface are followed by volatilization and expansion of the impact-produced cloud of refractory metals and, for the Ca bearing minerals at Mercury surface, the most likely involved compounds are $Ca(OH)_2$, CaOH, and/or CaO. The Ca atoms are produced via subsequent photolysis of these molecules considering the additional energy imparted to Ca products equal 0.9 eV, 0.3 eV, and 0.6 eV, respectively (Berezhnoy, 2018). The final products after the impact depend on the quenching temperature of the expanding cloud that is expected to be in the range 3000–4000 K. Exact temperature, photolysis lifetimes of the produced molecules and excess energy during different photolysis processes are still not well constrained by observations. At temperatures $\leq$3750 K in the impact-produced cloud $Ca(OH)_2$ dominates over both atomic Ca, CaO and CaOH, while at higher temperatures it is considered that the predominant form of the initial calcium ejecta is CaO (Berezhnoy, 2018). In this study, we examine MMIV processes in a different ranges of vapor cloud temperature and compare the results (section 4). In particular, a two-step process is suggested in which the initial Ca-bearing molecules ejection by MMIV is followed by a second process that dissociates these molecules, and produces highly energetic atomic Ca as observed during MASCS measurements.

The CaO molecules can be dissociated in the exosphere by different processes. It was shown that electron-impact dissociation cannot reproduce the observed Ca tangent column density of 5–15 $\cdot 10^8$ cm^{-2} as in Burger et al. (2014). In fact, by considering that solar wind electrons flux is estimated between 10^7 and 10^9 cm^{-2} s^{-1} (Gershman et al., 2015), the e-impact dissociation cross section is of the order of $0.4 \cdot 10^{-16}$ cm^2 at 1 keV (Miles, 2015) and the lifetime of neutral Ca as the photoionization lifetime at Mercury is between 1380 s at perihelion and 3120 s at aphelion. As a result, the column density of Ca would be $<10^5$ cm^{-2} (Killen, 2016), which is orders of magnitude too low compared with the observed Ca one. The spontaneous dissociation of CaO could also be a possible pathway for producing Ca, but the energy in the products is <1 eV/atom and is not enough to accelerate the atomic Ca to the altitudes where it is observed. The photodissociation of the released CaO molecules by MMIV could explain the dawn-dusk asymmetry of the exosphere, because the molecules are preferentially ejected into the

exosphere in the dawn side by impact vaporization and subsequently dissociated by photons. But it likely cannot energize the resulting Ca so that contributes for the low energy Ca component in the planetary exosphere. Hence, these processes are not good candidates to cause the release of energetic Ca into the Mercury exosphere.

Killen (2016) suggested that the most likely origin of extremely energetic Ca seen in Mercury's exosphere is CaO non- equilibrium dissociative ionization produced by impact vaporization, followed by neutralization of Ca^+.

Plainaki et al. (2017), starting from the same assumptions in Killen (2016), where only <1% of the vapor is ionized and dissociates, modeled the 3D distribution of the Ca exosphere after the crossing of the comet 2P/Encke dust stream. The simulated Ca distribution was consistent with the geometry and the vertical profile of the MESSENGER/ UVVS observations, but not with the intensity. In fact, the estimated Ca column abundance produced by shock-induced dissociative neutralization was $<4 \cdot 10^7$ cm^{-2}, lower than the observed one by up to 2 orders of magnitude. This disagreement is reasonably related to the uncertainty in the definition of some parameters and assumptions used in their model, as also suggested by the same authors (Plainaki et al., 2017). The strong dependence of some of the modeled quantities on specific input-parameters, which in turn describe the actual nature of the phenomenon in action, evidences the complexity in the interpretation of the Ca-observations. In addition to this, Berezhnoy (2018) analyzed the chemistry of formation of molecules and dust grains in the cloud produced after collisions by meteoroids: it was found that the molar fraction of Ca-containing species providing the relative atomic and molecular Ca component to be in ratio 1:3 at quenching temperature of 3000–3500 K if the initial temperature and pressure of the impact-produced cloud are 10,000 K and 10,000 bar, respectively.

3. Model

We present a Monte Carlo three-dimensional model of the Hermean exosphere, that considers all the major sources of generation and loss processes. The numerical model (Mura et al., 2007, 2009) (Virtual Activity (VA) SPIDER, Sun-Planet Interactions Digital Environment on Request, in Europlanet-2024 program) includes, among the processes responsible of the formation of such an exosphere, the following ones: ion sputtering, thermal desorption, photon-stimulated desorption and micro-meteoroids impact vaporization. The model computes single-particle trajectories to reconstruct the spatial distribution of some components of the neutral exosphere of Mercury. The trajectories of particles are calculated by using the full equation of motion, including gravity force in Mercury reference frame and radiation pressure acceleration.

The acceleration due to the radiation pressure acts differently over different species. It is believed to be crucial for Na, and negligible for Ca. Radiation pressure is a function of the photon flux, of the Solar photon scattering probabilities (g-value) and of the amount of Doppler shift out of the Fraunhofer features. This latter quantity is, in turn, dependent on the velocity of the particle with respect to the Sun (Smyth and Marconi, 1995). Hence, since Ca atoms in Mercury' exosphere are highly energetic, with an extreme velocity with respect to the planet (Burger et al., 2014), the Doppler shifts of the lines could be different than what it would be when Ca is at rest with respect to the planet. For this reason, we did include the radiation pressure calculation in our model, by using the values given by Killen et al. (2009, 2022) and Burger et al. (2012). In the model, in addition to the Ca resonance line at 422.7 nm, also the lines at 272.2 nm and 456.7 nm are included in the radiation pressure calculation although they contribute less to the total effect (Burger et al., 2012). As required, we calculate the acceleration due to the radiation pressure estimating it at each step of the test-particle trajectory. However, we concluded that this modelling effort produced very little refinement of the simulated Ca profiles (the difference between the Ca profiles with or without radiation pressure ranges from 0% at the surface up to ~14% at 3 Rm).

In the simulations, the energetic Ca atoms are generated by instantaneous process from dissociative recombination, so test particles are described in the same section as launched from the surface. Ca and O test particles, as products of CaO photo-dissociation, are initialized by assuming that the photolysis process results in an extra energy (details in section 3.1 and Table 2) which is translated into an excess velocity for Ca and for O in the rest frame of the original molecule. These two excess velocities are given a randomly chosen direction and are added to the velocity of the parent CaO molecule.

The test-particle trajectory ends at the surface of the planet or when it is too far from the planet, i.e. $r > 10$ Rm. The simulated trajectories are accumulated into a matrix to obtain the spatial and energy distributions of particles. Since the full trajectory of each test particle is accumulated in the grid, the model is essentially a steady-state model. This assumption is valid because the lifetime of a typical Ca atom (between 500 and 1000 s in our simulations) is shorter with respect to the variability of the external conditions (which are modulated only by the orbit of Mercury). The variability of surface or external conditions can be reproduced by changing parameters in the functions describing the source processes and, for each set of values, a different numerical simulation can be performed. In particular, it is possible to model the exosphere of Mercury for each source separately so that we can investigate the role of each physical source independently of the others. We trace the trajectories of one million test-particles for each run using classical equations of motion, including gravity in the Mercurian reference frame.

A weight is assigned to the test-particle and, each time a test-particle crosses a grid cell, it is accumulated in the result matrix. The weight factor assigned to the Monte Carlo test particle is also continuously controlled, along the trajectory, to take into account the processes of photodissociation and photoionization. At each time step, we calculate the probability for the Ca-bearing molecule to dissociate, according to the position of the test particle, in dayside or in nightside, and we change the weight accordingly. Finally, the Ca density inside each grid cell is calculated taking into account the number of test particles that have been accumulated in the cell, their weight factor, the time that each test particle actually experiences inside the cell and the volume of the cell.

3.1. Model assumptions

The numerical Ca abundance in the regolith is assumed to be equal to 3.5% atomic percent (Killen, 2016) and we also assume that all the Ca is bounded to O, as CaO. From the MESSENGER/X-Ray Spectrometer (XRS)-derived maps (Weider et al., 2015) it is evident that there are some regions where the content of Ca on the surface of Mercury can be as high as 0.07, but for simplicity we assume a homogenous value for Ca abundance.

We must consider that a fraction of Ca-containing species is in the gas phase and part is in the solid phase as dust. The ratio between content of species in the gas phase to the total amount of Ca-containing species in gas and solid phases, is estimated to be lower than 0.05 (Berezhnoy et al., 2011). From this percentage we evaluate the fraction of atomic Ca and molecular CaO involved in the different processes. The resulting components at quenching temperature are considered in the ratio of 1:3 (Berezhnoy, 2018).

We first assume an isotropic source of Ca over Mercury's surface, making a comparison between such source and data observations. Subsequently, we suppose an asymmetric particles precipitation as discussed in Pokorný et al. (2018) (Fig. 1). In their work they compute the total mass ejected via micro-meteoroids that impact the surface and, in this paper, we consider only the percentage of Ca bearing particle abundance. Then, we simulate the exospheric energetic Ca component generated by the shock-induced non-equilibrium dissociative ionization process followed by the neutralization.

The efficiency of the neutralization process decreases with decreasing temperature of vapor cloud, so the bulk of the process should

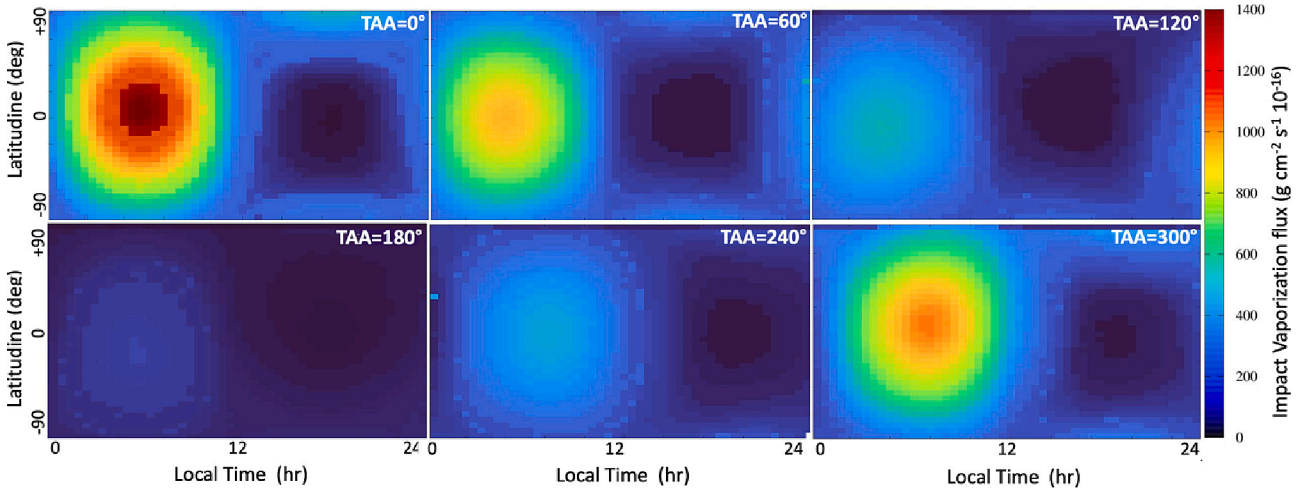

Fig. 1. Maps of impact vaporization flux for six different TAAs by Pokorný et al. (2018).

occur just after the initial impact, i.e. in timescales negligible with respect to cloud expansion (Killen, 2016). Hence, we assume that the velocity distribution of a fraction of total Ca immediately released to the exosphere during impacts of meteoroids is reproduced by the Maxwellian velocity distribution at 50,000 K (Burger et al., 2014).

The photo-dissociation of the CaO molecules generate the low energy Ca component. In this work we examine and compare two different studies: on the one hand, at quenching temperatures $\leq$ 3750 K $Ca(OH)_2$ dominates over both atomic Ca, CaO and CaOH (Berezhnoy, 2018) and it is valid to assume as the main Ca-containing compound in the impact-produced cloud. At 1 AU CaO pholotysis lifetime is estimated between 140 s and 3000 s (Valiev et al., *2017*); we adopted lifetime $\tau_{CaO} = 140$ s (Valiev et al., 2016; Berezhnoy, 2018) and we assume that the CaO in the exosphere is produced by a subsequent photolysis processes of $Ca(OH)_2$ and then CaOH (lifetime equal 2000 s and 600 s, respectively) (Berezhnoy, 2013, 2018). Starting from the photo-dissociation of these molecules, we estimate a final time of production of Ca atoms during photolysis of Ca-containing species $\tau_{Ca-bearing} \sim 270$ s, calculated at Mercury distance as the sum of scaled lifetimes of each reaction. This value is shorter than the ballistic time of molecules 760 *s* (Killen, 2016), so we aspect that the fraction of CaO molecules photolyzed is close to unity. In the model we consider the additional energy of Ca atoms during $Ca(OH)_2$, CaOH, and CaO photolysis (0.9 eV, 0.3 eV and 0.6, respectively) and the photodissociation of molecules would result in a total energy gain of about 1.8 eV for Ca (Berezhnoy, 2013, 2018). From these assumptions, a low energy Ca component is ejected with temperature equal ~20,000 K (details in Table 1).

On the other hand, at quenching temperatures $\geq$3750 K, we assume that the fraction of Ca-bearing particles is ejected as CaO at T ~ 4000 K. CaO lifetime is about $\tau_{CaO} \sim 10^4$ *s*,equal to the inverse of the photodissociation rate ($7.5\ 10^{-5}\ s^{-1}$ near the perihelion) and it is function of the orbital distance, and photodissociation of molecules would result in an energy gain of about 0.8 eV for Ca (Killen, 2016) (details in Table 2).

The Ca photoionization lifetime, τ_{Ca}, at Mercury varies from 1380 s at perihelion to 3120 s at aphelion (Burger et al., 2014) and in the current simulations we have assumed this parameter as a function of the orbital distance of the planet. A summary of the model assumptions is given in Table 3.

Table 1
Photolysis lifetimes τ(s) calculated at Mercury distance, energies and temperature of metal-containing products of photolysis of Ca-containing species. Assumptions from Berezhnoy (2013, 2018) and Valiev et al. (2016)

Molecules	*Reactions*	*Life time τ (s)*	*Energy (eV)*	*Temperature products (K)*
Quenching Temperature				≤3750
Ca(OH)2	$Ca(OH)_2 + h\nu = CaOH + OH$	200	0.9	~ 10,000
Ca(OH)	$CaOH + h\nu = CaO + H$	60	0.3	~ 3000
CaO	$CaO + h\nu = Ca + O$	14	0.6	~ 7000

4. Results and discussion

Fig. 2 shows the simplest case: the simulated CaO exosphere (left panel) released by micrometeoroids impacts and the subsequent Ca exosphere (right panel) generated from photodissociation of the molecules assuming that the precipitating particles have a uniform distribution on the surface. Our results suggest that an isotropic Ca source with temperatures of 50,000 K creates exospheres with densities up to $2{\cdot}10^6$ m^{-3} with a uniform distribution in the x-y plane, showing no dawn-dusk asymmetry, so it doesn't reproduce the spatial distribution that is observed by UVVS. An isotropic exospheric model, therefore, cannot actually describe the observed persistent, high-energy source of calcium, enhanced in the dawn equatorial region of Mercury, has to be considered, as previously suggested also by Burger et al. (2012).

Then, we consider a non-uniform precipitation of micrometeoroids to the planet surface and, as explained in the model assumptions (Section 3.1), we use Pokorný et al. (2018) maps of impact vaporization flux (Fig. 1) at different TAA in order to derive the released CaO and Ca components. In these maps, the most intense impact vaporization region is centered at the dawn terminator (~ 6 AM) both at perihelion and aphelion and it is slightly shifted when Mercury is moving along the orbit. The derived energetic Ca exosphere (T = 50,000 K) generated from the dissociative ionization and neutralization of Ca^+, for 4 different values of TAA, is presented in Fig. 3. Densities up to 10^6 m^{-3} are reproduced above the region of maximum emission located on dayside hemisphere, that shows an evident dawn-dusk asymmetry with highest

Table 2
Photolysis lifetimes τ (s) calculated at Mercury distance, energies and temperature of metal-containing products of photolysis of Ca-containing species. Assumptions from Killen (2016)

Molecules	*Reactions*	*Life time τ (s)*	*Energy (eV)*	*Temperature products (K)*
Quenching Temperature				≥3750
CaO	$CaO + h\nu = Ca + O$	10,000	0.8	~ 10,000

Table 3
Assumptions used for the simulated energetic Ca component derived from the dissociative ionization and neutralization of Ca^+ and the low energy Ca component generated by the photodissociation of the released Ca-bearing molecules. References: 1- assumptions of Killen (2016)

CaO and Ca Abundance		
Element Abundance	Value (%)	*References*
Surface composition Ca	3.5	Killen and Hahn (2015)
Ca-containing species gas phase	5	Berezhnoy et al. (2011)
Molecular Ca as CaO	75	Berezhnoy (2018)
Atomic energetic Ca	25	Berezhnoy (2018)
Parameters of processes responsible for Ca exosphere formation		
Energetic Ca component	*CaO component*	*Low energy Ca component*
	Cloud Quenching Temperature $\leq$ 3750 K	
T_{Ca} = 50,000 K	T_{CaO} = 13,000 K	T_{Ca} = 20,000 K
$t = t_0$*	$t = t_0$*	$t = t_0$* + 270 *s*
τ_{Ca}~*ns*	$\tau_{Ca-bearing}$~270 *s*	τ_{Ca}~*from* 1380 *s to* 3120*s*
Ca fraction at t_0 = 3.5% · 5% · 25%	CaO fraction at t_0 = 3.5% · 5% · 75%	
	Cloud Quenching Temperature $\geq$ 3750 K	
	T_{CaO} = 4000[1] K	T_{Ca} = 10,000 K
	$t = t_0$*	$t = t_0$* + 10 000 *s*
	τ_{CaO}~10 000[1] *s*	τ_{Ca}~*from* 1380 *s to* 3120*s*
	CaO fraction at t_0 = 3.5% · 5% · 75%	

*t_0 = *meteoroid impact time*

densities when Mercury is at perihelium.

We then simulate the low energy Ca component generated by photo-dissociation of molecules. We show in Fig. 4 the results obtained by assuming $Ca(OH)_2$ as the main Ca-containing compound in the impact-produced cloud. The CaO exosphere is produced as a product of the subsequent photolysis processes of $Ca(OH)_2$ in Ca(OH) and then in CaO. In this case, the CaO density is up to 10^7 m^{-3} above the surface in the dawn hemisphere where the molecules are preferentially ejected. The subsequent photo-dissociation of CaO that generates the Ca exospheric contribution at $T = 20{,}000$ K (Fig. 5) with densities up to 10^7 m^{-3}. The Ca enhancement is evident in the dawn-side where molecules are dissociated by sunlight and the trend of exospheric densities at different TAA shows the highest value at perihelion (TAA = 0°) near dawn and a minimum value at aphelion (TAA = 180°). We can observe a different spatial distribution of two Ca components (Figs. 3 and 5): while the energetic component is distributed in the whole hemisphere at dawn following the micrometeoroid's precipitation, the photodissociation process responsible of low energy Ca depends on sunlight and generates a denser exosphere in a smaller region, mainly at post-dawn.

The 3D plot in Fig. 6 shows the global Ca exosphere as the sum of both components, giving an overview of planet environment. There is an evident dawn-dusk asymmetry, as seen from the top-right figure (panel A) and from the midnight view (panel C), in agreement with the MESSENGER results; from dawn view (panel B), we can note that there is an enhancement in the post-dawn side where the two components maximize.

In Fig. 7 we plotted the vertical profile of total CaO and Ca components in the interval 1–3 Rm at TAA = 0° above the dawn terminator making a comparison between simulation results obtained with assumption of quenching temperature of the cloud $\leq$ 3750 K (left panel) with the study at higher temperatures (> 3750) (right panel). In the former, it can be noted that the low energy Ca component, produced by the subsequent photolysis processes, dominates over the other at low altitudes (up to 2 Rm) but the trend changes at higher Rm values showing that the energetic Ca generated by the non-equilibrium dissociative ionization and neutralization processes becomes denser. The

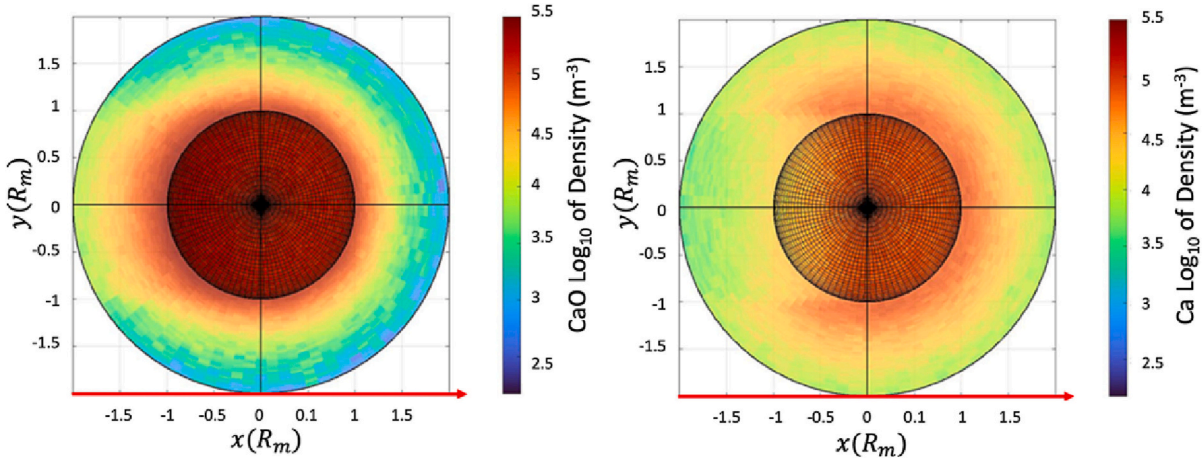

Fig. 2. Simulations of CaO (left) and energetic Ca (right) exospheres at TAA = 0° by micrometeoroid impacts assuming a uniform distribution of the ejected species. The x and y axes are oriented according to the Mercury Solar Orbital (MSO) coordinate system. In this MSO frame, x is directed from the planet's center to the Sun (red arrow), y is in the plane of Mercury's orbit and positive opposite to the planetary velocity vector, and z is positive toward north. (For interpretation of the references to colour in this figure legend, the reader is referred to the web version of this article.)

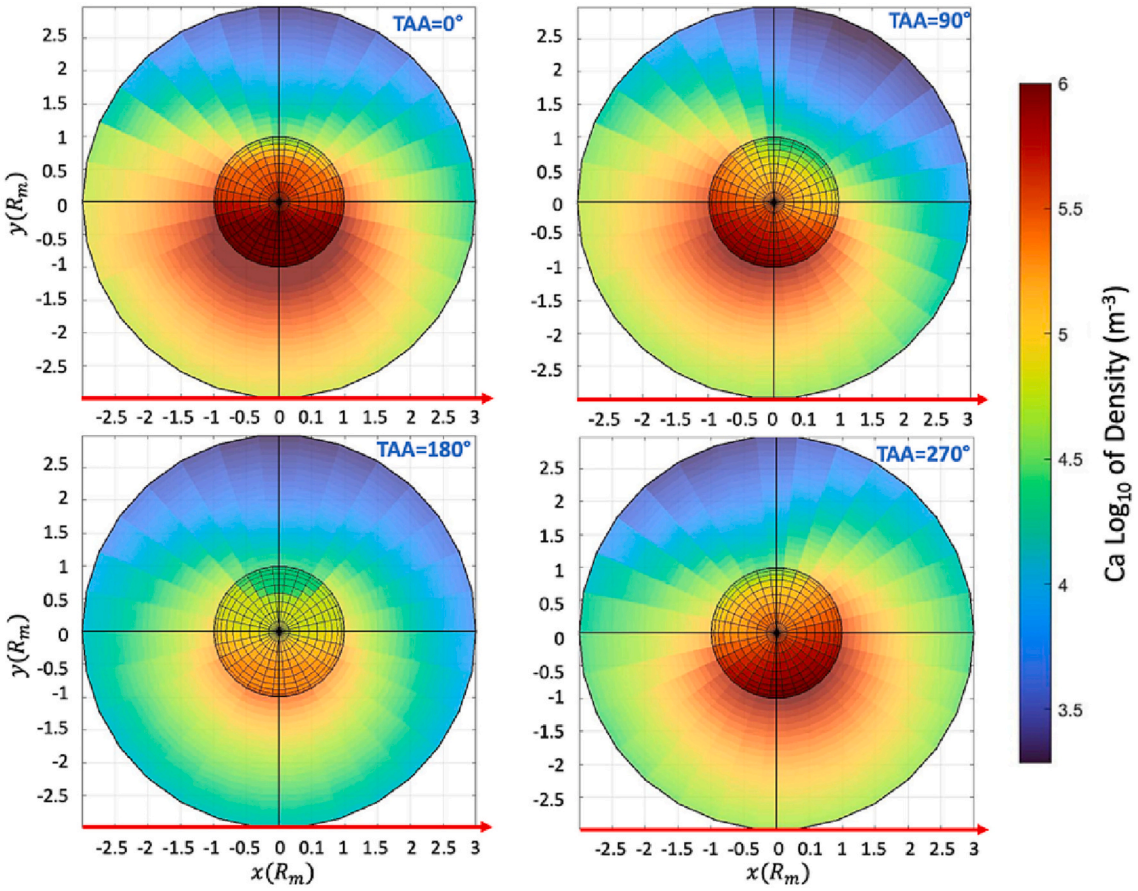

Fig. 3. Energetic Ca component at T = 50,000 K at different TAA (0°, 90°, 180° and 270°) generated through impact vaporization and subsequent dissociative ionization and neutralization of Ca^+, assuming an anisotropic precipitation of meteoroids. The x and y axes are oriented according to the MSO coordinate system (see Fig. 2 caption).

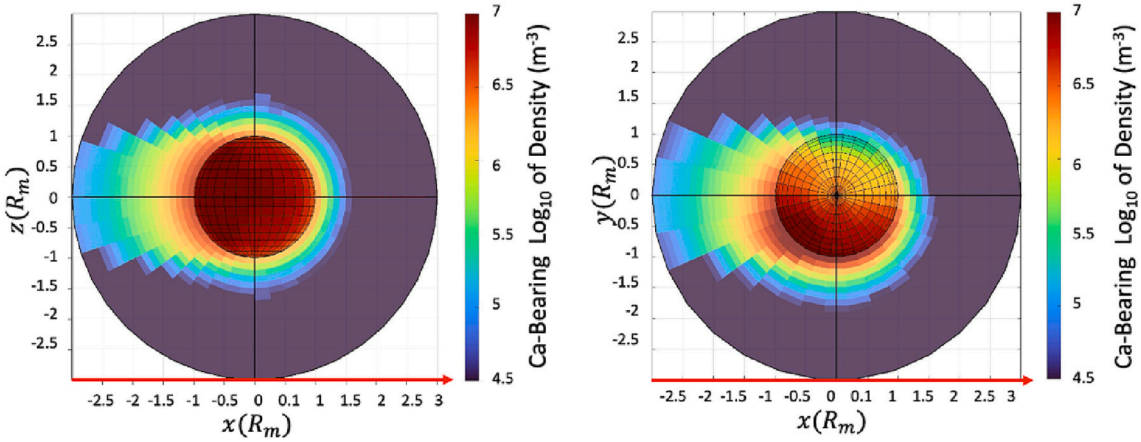

Fig. 4. Spatial distribution of Ca-bearing molecular densities at TAA = 0° generated by MMIV, assuming an anisotropic precipitation of meteoroids (as in Fig. 1). The x and y axes are oriented according to the MSO coordinate system (see Fig. 2 caption). Left panel reproduces the dawn hemisphere of CaO exosphere and right panel shows the north pole of planet.

resulting Ca exosphere is composed by two distinct populations at energy about 20.000 K and 50.000 K. Instead, in the right panel, the exosphere due to energetic Ca is denser that the low energy Ca at all altitudes, thus the Ca exosphere has a single predominant component, and the CaO exospheric profile is steeper.

Finally, our results of the MMIV-generated Ca exosphere are compared to the total Ca component as produced by the different processes with the profile by Burger et al. (2014) obtained through a best fit to the UVVS observations over two years (March 2011–2013). If we plot the seasonal dependence of total Ca content in the exosphere (Fig. 8), model results are consistent with the UVVS observations in the approximation of a temperature cloud $\leq$ 3750K (red line). At the contrary, the Ca exosphere estimation with higher temperature assumptions (purple line) shows results lower by a factor of 2 than the one obtained by Burger et al. (2014). The plots reproduce a peak at perihelium and a minimum value at aphelion. At aphelion photon flux is minimum,

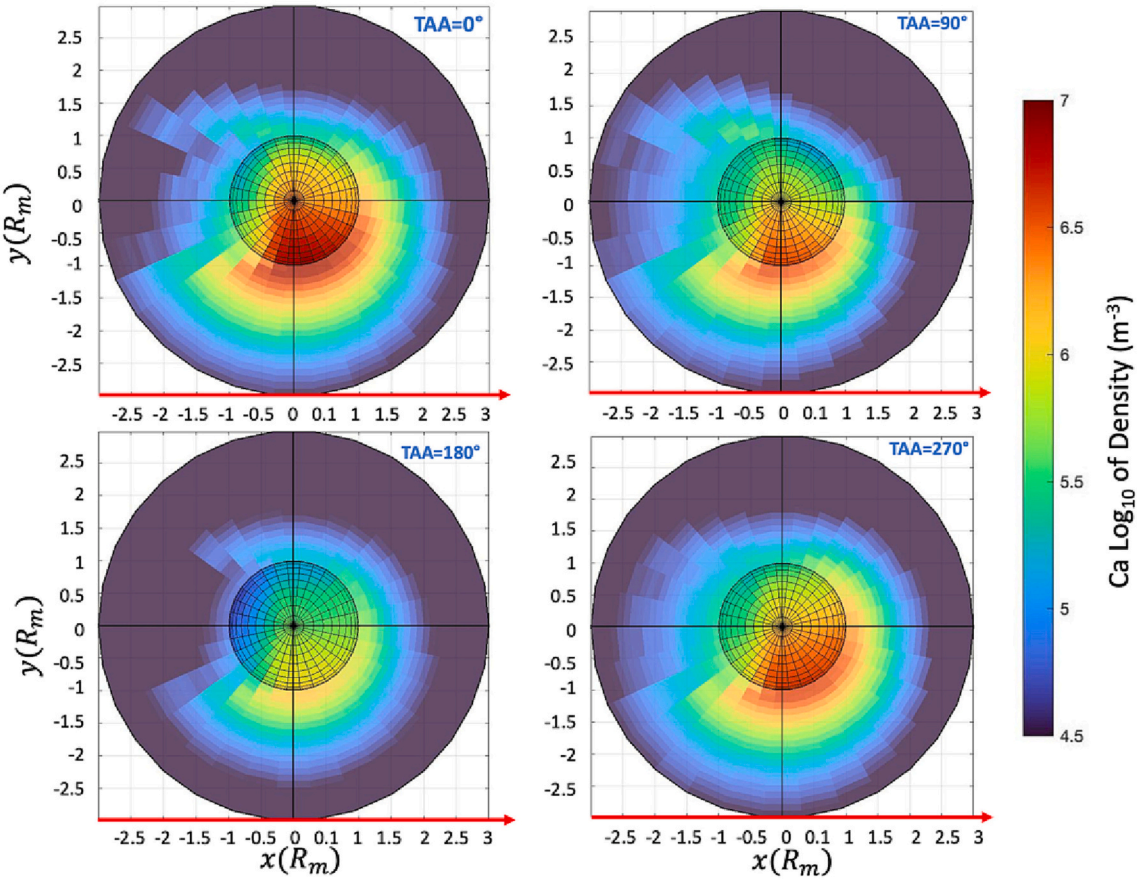

Fig. 5. The low energy Ca exosphere of Mercury at different TAA generated through the photodissociation of the CaO component. The x and y axes are oriented according to the MSO coordinate system (see Fig. 2 caption).

decreasing with the inverse square root of the distance, so that the Ca lifetime in the exosphere is the longest (lower photoionization) and the efficiency of photodissociation of CaO is the lowest. In the same orbit position, also the micrometeoroid flux is minimum, so that also Ca production via MMIV is the lowest. In the end, we have a combination of all these factors, a lower production rate and a lower loss rate. The final result is a less dense Ca exosphere. The excess emission in the plot by Burger et al. (2014) near TAA ~25° was attributed to the vaporization of surface material induced by the impact of a meteor stream, possibly resulting from Comet Encke (Killen and Hahn, 2015). Plainaki et al. (2017) studied the bombardment of the surface by particles from comet 2P/Encke simulating the expected 3-D spatial distribution of Mercury's Ca exosphere, but in present work we don't consider this contribution for the MMIV process.

5. Conclusions

In this paper we investigate and study the Micro-Meteoroids Impact Vaporization process as source of Mercury's Ca exosphere through the Monte Carlo 3D model simulations of the Hermean exosphere (Mura et al., 2007).

First of all, we verify that a uniform meteoroid precipitation cannot reproduce the dawn–dusk asymmetry observed in-situ in the Ca exosphere with the MESSENGER/MASCS sensor. The hypothesis of an asymmetric precipitation of micro-meteoroids that is higher in the dawn side (as from Pokorný et al. (2018)) is needed to explain the observed distribution. The derived CaO exospheric densities are up to 10^7 m^{-3} maximizing on the dawn-side hemisphere, that is where the dust preferentially impacts the planet's surface. Following previous studies (Killen, 2016; Plainaki et al., 2017), we consider that the atomic Ca in Mercury's exosphere may be produced in a sequence of different processes: the exospheric energetic Ca component derives from the shock-induced non-equilibrium dissociative ionization and neutralization of Ca^+ during the vapor cloud expansion, while a low energy Ca component is generated later by the photo-dissociation of the CaO molecules released by micro-meteoroid impact vaporization.

We simulate the MMIV process comparing two different set of parameters: in the approximation of a vapor cloud quenching temperature $\leq$ 3750 K, we suppose that the CaO in the exosphere is produced by a subsequent photolysis processes of Ca(OH)2, the dominant compound, and then Ca(OH) and finally CaO; in a second case, we simulated the Ca exosphere assuming CaO as the predominant form of the initial Ca-bearing molecules ejecta at $\geq$ 3750 K, as considered in previous papers, like Killen et al. 2016 and Plainaki et al., 2017. We simulated total Ca distribution in terms of atoms in the exosphere at different TAAs to reproduce the exospheric variability along the planet orbit and compared the results with the MESSENGER/MASCS observations by excluding the contributions due to possible comet streams (Fig. 8). We lead to a conclusion that theoretical calculations agree better with observations at shorter photolysis lifetimes and higher excess energy of Ca atoms obtained during photolysis of Ca-bearing species. In that case we can emphasize the presence of two different Ca components where the energetic Ca component is more intense than the other at high altitudes, but in the post-dawn low altitudes we can see a substantial contribution of the low energy component to the global Ca exospheric content, as shown in Figs. 6 and 7.

In the present work we focused on Ca Mercury exosphere reconstruction, but to obtain a more detailed description of the Ca-bearing exospheric components in the future, we will make a detailed study of the behavior of different Ca-containing species considering the lifetimes

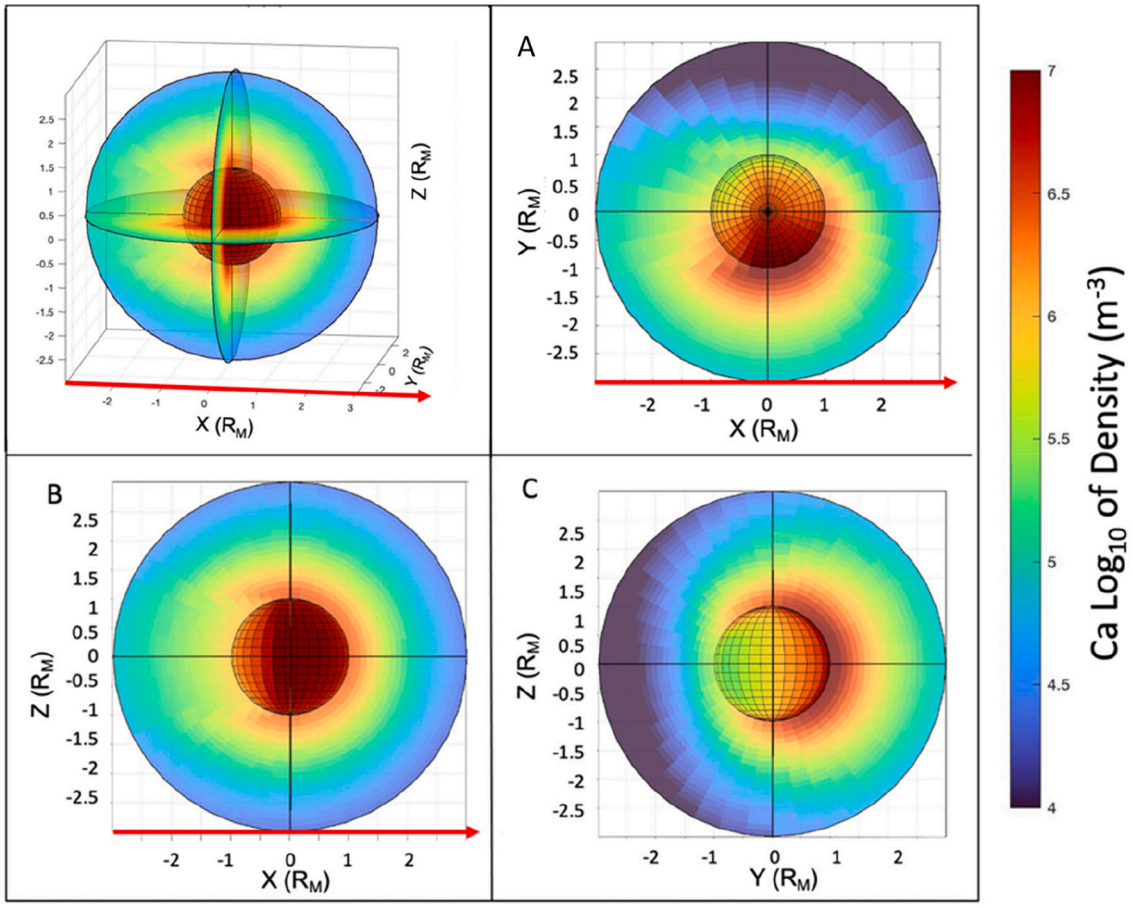

Fig. 6. 3D plot of Ca exosphere considering the contributions of both Ca components at perihelion. Panel A-B-C represent the projection of planet's exosphere along the direction x-y-z oriented according to the MSO coordinate system (see Fig. 2 caption); red line points to the Sun. (For interpretation of the references to colour in this figure legend, the reader is referred to the web version of this article.)

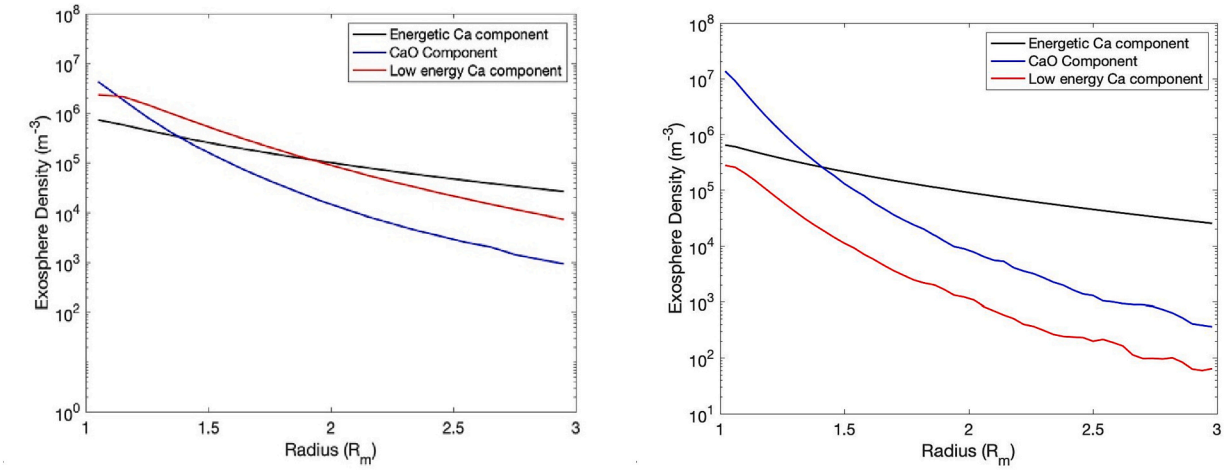

Fig. 7. Vertical density profiles of the CaO and the Ca components in the range up to 2 Rm (Mercury radii) above the surface, at perihelion (TAA = 0°) assuming a vapor cloud quenching temperature ≤3750 K (left panel) and > 3750 K (right panel).

and ballistic trajectories after the photodissociation processes. We also plan to add the simulation of the bombardment of planet surface by particles from cometary streams, in particular the crossing of Mercury's orbital plane and comet 2P/Encke that could justify the enhancement in Ca exosphere after perihelion (Killen and Hahn, 2015; Christou et al., 2015).

Since the MMIV contribution in refilling the exosphere is strongly dependent by impact velocity and size of the meteoroids, as future work we aim to combine different sources of meteoroids in the Solar System considering the different impact flux map (Pokorný et al., 2018) that describe the relative contributions of these populations to the planet's exosphere.

We could also consider different surface mineralogy, for example by considering that not all the Ca atoms are bounded to Oxygen but a

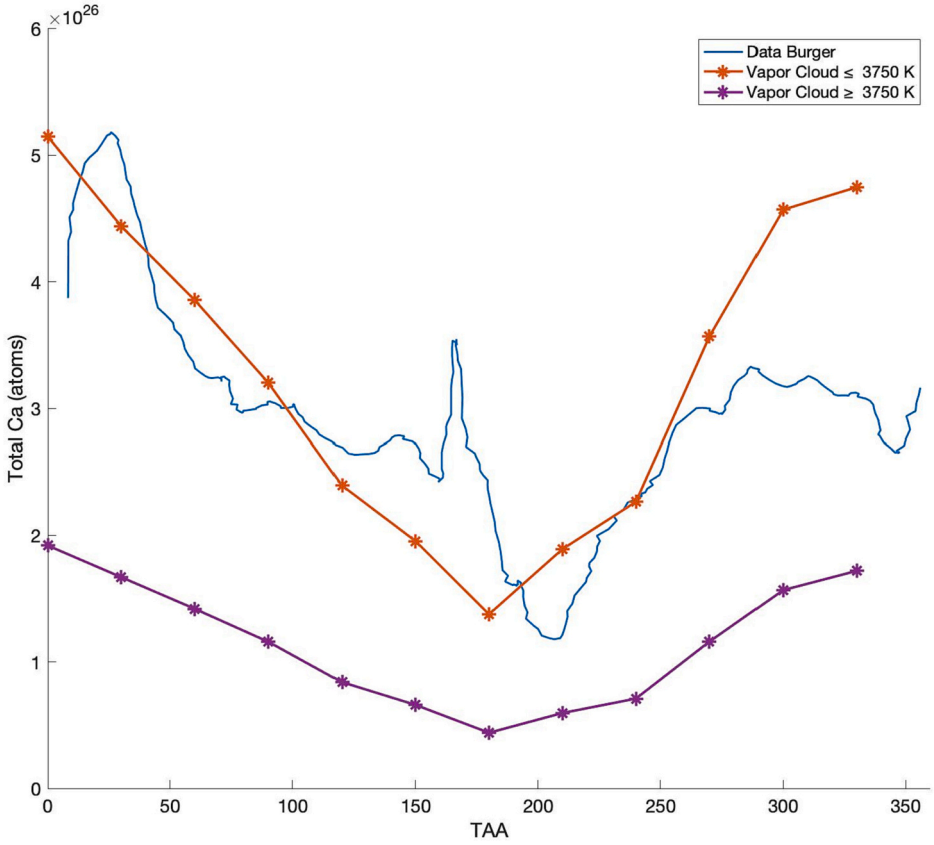

Fig. 8. Comparison between the simulations results obtained in the approximation of temperature vapor cloud ≤3750 K (red line) and at higher temperatures (yellow line) with the observations (Burger et al., 2014; blue line) along the orbit and, hence, True Anomaly Angle (TAA). (For interpretation of the references to colour in this figure legend, the reader is referred to the web version of this article.)

fraction of it could be bounded to Sulfur (CaS) or to OH. In those cases, different time scales of photolysis of different Ca-containing species could produce slightly different exosphere Ca distributions. We could also consider realistic surface composition mapping from MESSENGER measurements (Weider et al., 2015; Nittler et al., 2011).

Finally, other exospheric species are expected to be released by MMIV process; first of all, MESSENGER/MASCS detected also energetic Mg component, that shows a distribution quite similar to the Ca one (Sarantos et al., 2011). Therefore, in the future we wish to simulate other expected exospheric components.

This study is a meant to be a step forward in the understanding of the MMIV process at Mercury; furthermore, the model is a strong and useful tool to the scientific community for the interpretation for data as well a for observational strategies of the ESA/JAXA BepiColombo mission, that will start its nominal mission phase in *2026*. In particular, the resulting molecular distributions will be compared to the measurements of the MPO/SERENA-STROFIO mass spectrometer that will be the only instrument able to identify the molecular components, as CaO, and will permit to obtain simultaneous observations of different molecular and atomic components of the exosphere. These measurements coupled with the dust measurements by Mio/MDM instrument will allow for the first time a full investigation of the effect of MMIV at a planet.

Declaration of Competing Interest

The authors declare that they have no known competing financial interests or personal relationships that could have appeared to influence the work reported in this paper.

Data availability

I have shared the link to the on line tool at the attach file step

Acknowledgements

This work has been supported by the ASI-INAF agreement no. 2018-8-HH.1-2022 “Partecipazione scientifica alla missione BEPICOLOMBO SERENA Fase El” and Addendum.

The Sun Planet Interactions Digital Environment on Request (SPIDER) Virtual Activity of the Europlanet H2024 Research Infrastucture is funded by the European Union’s Horizon 2020 research and innovation programme under grant agreement No 871149 (*https://www.europlanet-society.org/europlanet-2024-ri/spider/*).

References

Berezhnoy, A.A., 2013. Chemistry of impact events on the Moon. Icarus 226, 205–211.
Berezhnoy, A.A., 2018. Chemistry of impact events on Mercury. Icarus 300, 210–222.
Berezhnoy, A.A., Mangano, V., Mura, A., Milillo, A., Orsini, S., 2011. Density distribution of metal-containing species in the exosphere of Mercury after meteoroids impacts. In: EPSC Abstracts, Vol. 6, EPSC-DPS2011–1793, 2011, EPSC-DPS Joint Meeting 2011.
Bida, T.A., Killen, R.M., Morgan, T.H., 2000. Discovery of calcium in Mercury’s atmosphere. Nature 404 (9), 159–161.
Burger, M.H., Killen, R.M., McClintock, W.E., Vervack, R.J., Merkel, A.W., Sprague, A.L., Sarantos, M., 2012. Modeling MESSENGER observations of calcium in Mercury’s exosphere. J. Geophys J. Res. 117.
Burger, M.H., Killen, R.M., McClintock, W.E., et al., 2014. Seasonal variations in Mercury’s dayside calcium exosphere. Icarus 238, 51–58.
Ceplecha, Z., 1992. Influx of interplanetary bodies onto Earth. Astron. Astrophys. 263 (1–2), 361–366.
Christou, A.A., Killen, R.M., Burger, 2015. The meteoroid stream of comet Encke at Mercury: Implications for MErcury Surface, Space ENvironment, GEochemistry, and Ranging observations of the exosphere. Geophys. Res. Lett. 42, 7311–7318.

Cintala, 1992. Impact-induced thermal effects in the lunar and Mercurian regoliths. J. Geophys. Res. 97, 947–973.
Gershman, D.J., Raines, J.M., Slavin, J.A., Zurbuchen, T.H., Anderson, B.J., Korth, H., Ho, G.C., Boardsen, S.A., Cassidy, T.A., Walsh, B.M., Solomon, S.C., 2015. MESSENGER observations of solar energetic electrons within Mercury's magnetosphere. J. Geophys. Res. Space Physics 120, 8559–8571.
Killen, R.M., 2016. Pathways for energization of ca in Mercury's exosphere. Icarus 268, 32–36.
Killen, R.M., Hahn, J.M., 2015. Impact vaporization as a possible source of Mercury's calcium exosphere. Icarus 250, 230–237.
Killen, R.M., Potter, A.E., Vervack, R.J., Bradley, E.T., McClintock, W.E., Anderson, C.M., Burger, M.H., 2010. Observations of metallic species in Mercury's exosphere. Icarus 209, 75–87.
Killen, R.M., Shemansky, D., Mouawad, N., 2009. Expected emission from Mercury's exoshperic species, and their ultraviolet-visible signatures. ApJS 181, 351.
Killen, R.M., Vervack, R.J., Burger, M.H., 2022. Updated photon scattering coefficients (g_values) for Mercury's exospheric species. ApJS 263, 37.
Kurosawa, K., 2012. Shock-induced silicate vaporization: the role of electrons. J. Geophys. Res. 117.
Mangano, V., Milillo, A., Mura, A., Orsini, S., De Angelis, E., Di Lellis, A.M., Wurz, P., 2007. The contribution of impulsive meteoritic impact vaporization to the Hermean exosphere. Planet. Space Sci. 55 (11), 1541–1556.
Marchi, S., Morbidelli, A., Cremonese, G., 2005. Flux of meteoroid impacts on Mercury. Astron. Astrophys. 431 (I. 3), 1123–1127.
McClintock, W.E., Lankton, M.R., 2007. The Mercury atmospheric and surface composition spectrometer for the MESSENGER mission. Space Sci. Rev. 131 (1–4), 481–521.
Merkel, A.W., Cassidy, T.A., Vervack, R.J., McClintock, W.E., Sarantos, M., Burger, M.H., Killen, R.M., 2017. Seasonal variations of Mercury's magnesium dayside exosphere from MESSENGER observations. Icarus 281, 46–54.
Miles, P., 2015. Study of Mercury's Neutral Molecular Exosphere. PhD Dissertation,. University of Texas at San Antonio.
Milillo, A., Fujimoto, M., Murakami, G., Benkhoff, J., Zender, J., Aizawa, S., Dósa, M., Griton, L., Heyner, D., Ho, G., et al., 2020. Investigating Mercury's environment with the two-spacecraft BepiColombo mission. Space Sci. Rev. 216 (5), 1–78.
Milillo, A., Wurz, P., Orsini, S., Delcourt, D., Kallio, E., Killen, R.M., Lammer, H., Massetti, S., Mura, A., Barabash, S., Cremonese, G., Daglis, I.A., De Angelis, E., Di Lellis, A.M., Livi, S., Mangano, V., Torkar, K., 2005. Surface-exosphere-magnetosphere system of Mercury. Space Sci. Rev. 117 (3), 397–444.
Mura, A., Milillo, A., Orsini, S., Massetti, S., 2007. Numerical and analytical model of Mercury's exosphere: dependence on surface and external conditions. Planet. Space Sci. 55, 1569–1583.
Mura, A., Wurz, P., Lichtenegger, H.I.M., Schleicher, H., Lammer, H., Delcourt, D., Milillo, A., Orsini, S., Massetti, S., Khodachenko, M.L., 2009. The sodium exosphere of mercury: comparison between observations during Mercury's transit and model results. Icarus 200, 1–11.
Nesvorný, D., Jenniskens, P., Levison, H.F., Bottke, W.F., Vokrouhlický, D., Gounelle, M., 2010. Cometary origin of the zodiacal cloud and carbonaceous micrometeorites. Implications for hot debris disks. Astrophys. J. 713, 816–836.
Nesvorný, D., Janches, D., Vokrouhlický, D., Pokorný, P., Bottke, W.F., Jenniskens, P., 2011. Dynamical model for the zodiacal cloud and sporadic meteors. Astrophys. J. 743, 129.
Nittler, L.R., et al., 2011. The major-element composition of Mercury's surface from MESSENGER X-ray spectrometry. Science 333, 1847–1850.
Plainaki, C., Mura, A., Milillo, A., Orsini, S., Livi, S., Mangano, V., Massetti, S., Rispoli, R., De Angelis, E., 2017. Investigation of the possible effects of comet Encke's meteoroid stream on the Ca exosphere of Mercury. J. Geophys. Res. Planets 122, 1217–1226.
Pokorný, P., Sarantos, M., Janches, D., 2018. A comprehensive model of the meteoroid environment around Mercury. Astrophys. J. 863 (1), 31.
Sarantos, M., Killen, R.M., McClintock, W.E., Todd Bradley, E., Vervack, R.J., Benna, M., Slavin, J.A., 2011. Limits to Mercury's magnesium exosphere from MESSENGER second flyby observations. Planet. Space Sci. 59, 1992–2003.
Seki, K., Nagy, A., Jackman, C.M., Crary, F., Fontaine, D., Zarka, P., Wurz, P., Milillo, A., Slavin, J.A., Delcourt, D.C., Wiltberger, M., Ilie, R., Jia, X., Ledvina, S.A., Liemohn, M.W., Schunk, R.W., 2015. A review of general physical and chemical processes related to plasma sources and losses for solar system magnetospheres. Space Sci. Rev. 192, 27–89.
Smyth, W.H., Marconi, M.L., 1995. Theoretical overview and modeling of the sodium and potassium atmospheres of Mercury. Astrophys. J. 441, 839–864.
Solomon, S.C., Anderson, B.J., 2018. The MESSENGER mission: Science and implementation overview. In: Solomon, S.C., Nittler, L.R., Anderson, B.J. (Eds.), Mercury the View after MESSENGER. Cambridge University Press, Cambridge.
Valiev, R.R., Berezhnoy, A.A., Minaev, B.F., Chernov, V.E., Cherepanov, V.N., 2016. Ab initio study of electronic states of astrophysically important molecules. Russ. Phys. J. 59, 536–543.
Valiev, R.R., Berezhnoy, A.A., Sidorenko, A.D., Merzlikin, B.S., Cherepanov, V.N., 2017. Photolysis of metal oxides as a source of atoms in planetary exospheres. Planet. Space Sci. 145, 38–48.
Weider, S.Z., et al., 2015. Evidence for geochemical terranes on mercury: global mapping of major elements with MESSENGER's X-ray spectrometer. Earth Planet. Sci. Lett. 416, 109–120.
Wurz, P., Lammer, H., 2003. Monte-Carlo simulation of Mercury's exosphere. Icarus 164, 1–13.